FULL PAPERS

Magnetic Resonance in Medicine 000:000–000 (2010)

Comparison of the Quantitative First Pass Myocardial Perfusion MRI With and Without Prospective Slice Tracking: Comparison Between Breath-Hold and Free-Breathing Condition

Dirk Ernst Johannes Cleppien,[1] Georg Horstick,[2] Nico Abegunewardene,[2] Stefan Weber,[1] Christian Ernst Müller,[1] Axel Heimann,[3] Karl-Friedrich Kreitner,[4] Oliver Kempski,[3] and Laura Maria Schreiber[1]*

Physiologic motion of the heart is one of the major problems of myocardial blood flow quantification using first pass perfusion–MRI method. To overcome these problems, a perfusion pulse sequence with prospective slice tracking was developed. Cardiac motion was monitored by a navigator directly positioned at heart's basis to overcome no additional underlying model calculations connecting diaphragm and cardiac motion. Additional prescans were used before the perfusion measurement to detect slice displacements caused by remaining cardiac motion between navigator and the perfusion slice readout. The pulse sequence and subsequent quantification of myocardial blood flow was tested in healthy pigs with and without prospective slice tracking under both free-breathing and breath-hold conditions. To avoid influences by residual contrast agent concentration time courses were analyzed. Median myocardial blood flow values and interquartile ranges with prospective slice tracking under free-breathing and in a breath-hold were (1.04, interquartile range = 0.58 mL/min/g) and (1.20, interquartile range = 0.59 mL/min/g), respectively. This is in agreement with published positron emission tomography values. In measurements without prospective slice tracking (1.15, interquartile range = 1.58 mL/min/g), the interquartile range is significantly ($P < 0.012$) larger because of residual cardiac motion. In conclusion, prospective slice tracking reduces motion-induced variations of myocardial blood flow under both during breath-hold and under conditions of free-breathing. Magn Reson Med 000:000–000, 2010. © 2010 Wiley-Liss, Inc.

Key words: magnetic resonance imaging; myocardial perfusion; quantitative myocardial blood flow; prospective slice tracking

Many diseases of the heart have a significant influence on myocardial blood flow (MBF). A recent study has shown (1) that the MBF decreases in case of a severe stenosis of a coronary artery. Therefore, it is an important diagnostic step to quantify the MBF accurately to obtain valid information about the status of the myocardial microcirculation.

The noninvasive clinical gold standard is $H_2^{15}O$- or $^{13}NH_3$-positron emission tomography (PET) (1). A recent study applying this method (2) states that the resting MBF ranges from 0.59 to 2.05 mL/min/g (average, 0.98 ± 0.23 mL/min/g) in healthy humans. Gold standard for experimental MBF measurements are radio labeled microspheres, where the MBF is quantified after histological work-up of the tissue (3).

Another approach is the dynamic first pass perfusion (FPP)–MRI (4). Here, the first pass of a T_1-shortening contrast agent (CA) is measured over time. Similar to the PET-method, the quantitative MBF is calculated by applying mathematical models to the measured signal time courses (STCs) in myocardial tissue. The advantages of FPP–MRI over PET are its high spatial and temporal resolution in combination with a sufficient image contrast, the absence of radioactive tracers and its better acceptance by patients. However, cardiac motion during the dynamic measurement, e.g., because of a suboptimal breath-hold or changes of lung volume due to oxygen consumption during the measurement, is a problem in a significant number of studies because this motion renders reliable measurements of STCs almost impossible. STCs may appear correctly derived but an unclear prior history of radio frequency excitations, an undefined volume of signal generation and an increase in partial volume effects may render the results unusable although there may be no evidence about this in the MRI data. It should be mentioned that perfusion measurements with PET also suffer from cardiac motion, but the influence is neglected in the standard approach because of the long measurement time and the relatively poor spatial resolution.

One of the common approaches to account for the heart's motion is navigator-based MRI. Here, it is assumed that the motion of the heart correlates with diaphragm motion. However, the deviation between cardiac motion and the movement of the diaphragm is

[1]Section of Medical Physics, Department of Radiology, Johannes Gutenberg University Medical Center Mainz, Mainz, Germany.

[2]Department of Cardiology, Johannes Gutenberg University Medical Center Mainz, Mainz, Germany.

[3]Department of Neurosurgical Pathophysiology, Johannes Gutenberg University Medical Center Mainz, Mainz, Germany.

[4]Department of Radiology, Johannes Gutenberg University Medical Center Mainz, Mainz, Germany.

Grant sponsor: German Research Foundation (DFG); Grant number: SCHR 687/1; Grant sponsor: MAIFOR Mainz (Germany); Grant sponsor: Robert-Mueller-Stiftung Wiesbaden (Germany).

*Correspondence to: Laura Maria Schreiber, PhD, MBA, Section of Medical Physics, Department of Radiology, Johannes Gutenberg University Medical Center, Langenbeckstrasse 1, 55131 Mainz, Germany. E-mail: lschreib@uni-mainz.de

Received 6 November 2009; revised 22 April 2010; accepted 24 April 2010.

DOI 10.1002/mrm.22513

Published online in Wiley InterScience (www.interscience.wiley.com).

individual for every patient and needs to be measured on an individual patient basis. The resulting slice shift can be compensated for in three different ways. In the first approach, only slices measured at the same position of the diaphragm are combined after the measurement during image reconstruction (retrospective gating) (5). In the second, a slice will only be measured if the diaphragm is in the preselected position (prospective gating), an approach not compatible with FPP–MRI of the heart. In the third technique, also called prospective slice tracking (PST) (6,7), the slice position is continuously monitored by the pulse sequence and adapted to the diaphragm position during the MRI measurement.

For FPP–MRI, only the third approach is of use because only this method offers a sufficient temporal resolution to measure the STCs precisely. Pedersen et al. (8) used this approach under free-breathing conditions and their result was a decrease of in-plane motion as a result of reduced through plane (TP) motion. This also significantly reduced the mean perfusion error of calculated perfusion values measured with PST compared with the mean error of the values obtained in the measurements without PST.

The aim of this study was to develop a navigator-based FPP–MRI method with PST for quantitative MBF measurements in units of milliliters per minute per gram. The navigator was positioned perpendicular to the corresponding perfusion slice across the heart. The advantage of this approach is that cardiac motion is measured directly to overcome the standard motion detection approach with its pitfalls of additional underlying model calculations connecting diaphragm and cardiac motion. Furthermore, we determined the benefit of PST for quantitative MBF measurements at rest against measurements without PST. This was done by comparing PST under both free-breathing and breath-hold conditions to measurements without PST in an animal study.

MATERIALS AND METHODS

General Experimental Setup

All experiments were performed on a 1.5 T clinical whole-body cardiovascular MRI System (Magnetom Sonata, Siemens Medical Solution, Erlangen, Germany). The MRI system is equipped with high-performance gradients (slew rate 200 mT/m/sec; peak amplitude 40 mT/m). For data acquisition, a six-element phased array cardiac coil was used in combination with two elements of the spine array.

Pulse Sequence

For perfusion imaging combined with PST, an in-house developed saturation recovery TurboFLASH (SRTF) sequence was used. The sequence acquired one image of the slice with navigator-based PST and subsequently one without PST within every heartbeat to acquire both corrected and uncorrected STCs under almost the same physiological conditions (cf. Fig. 1). For clinical measurements, however, the measurements without PST would be dropped. For PST, high-resolution spin-echo navigator echoes (9) were used to monitor cardiac

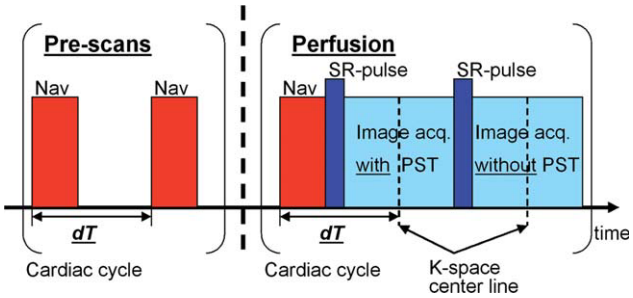

FIG. 1. Timing diagram of the SRTF sequence with PST. [Color figure can be viewed in the online issue, which is available at www.interscience.wiley.com.]

motion during measurement by observing the heart-lung interface at the basis of the heart.

For this purpose, the following problems had to be solved:

- First of all, the influence of the navigator signal on signal intensity (SI) of the perfusion slice due to its positioning over the heart could be ignored by using a saturation recovery perfusion pulse sequence (time of saturation pulse combined with subsequent gradient spoiling $t_{\text{Sat-Modul}} = 12.56$ msec). The saturation pulse spoils all spins in the measurement volume and therefore suppresses possible artifacts of the navigator excitation in the perfusion slice image. This was tested in the phantom with the relaxation times compared with the myocardium as described below and no unwanted side effects were observed.
- Second, for accurate motion detection at the heart due to its shape and relatively small volume extension in contrast to the diaphragm, a navigator with high spatial resolution was essential. However, this usually presents with low signal-to-noise ratio (SNR). The quality of motion detection is also related to the contrast-to-noise ratio (CNR) between the SI of those areas not moving and those moving. In this study, we found a sufficient CNR for the detection of cardiac motion by using a navigator signal, which was interpolated by a factor of 2, Hamming filtered, all recorded channels of the coils were combined, signal magnitude was reconstructed by Fourier transformation (spatial resolution = 0.37 mm^2, slice thickness = 6–7 mm) and spatially averaged using a median filter with a length of six pixels.
- Third, the influence of CA wash-in into the lung, which also reduces the CNR between lung and heart tissue and therefore the detectability of the interface between both tissues, was also reduced to a negligible amount by using optimized echo time (TE). For optimization, we first investigated the dependency of CNR between myocardium and tissues with varying amount of CA on TE in a simulation, based on the spin echo signal equation (10), $T_{1,\text{myocardium}} = 880$ msec (11), $T_2 = 75$ msec (11), and TR = 460 msec (time between T_1-saturation of perfusion slice readout and navigator excitation, heartbeat rate=800 msec). Then, we optimized TE in phantoms as described below and validated the optimized TE in vivo during perfusion measurements.
- Fourth, the motion of the interface between the heart and the lung had to be detected and, if

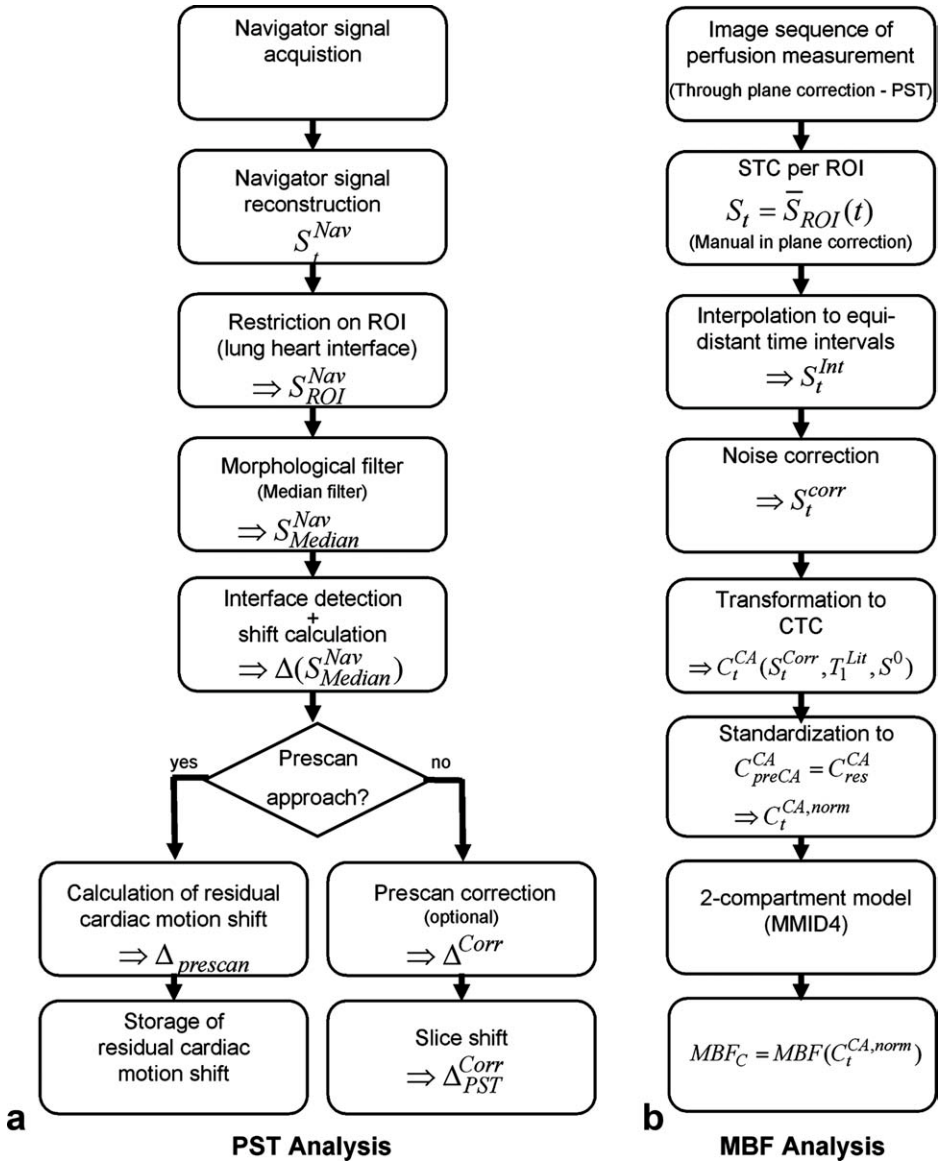

FIG. 2. Flowcharts for data analysis of (for details see text): (**a**) navigator-based PST; (**b**) perfusion measurement in the animal study.

necessary, the position of the perfusion slice had to be corrected in real time (cf. Fig. 2). The motion detection was performed adjustable due to the contrast changes of the tissues during bolus passage of CA. The position of the heart's interface to the lung was located at that pixel in the navigator's signal magnitude, where the SI passed half of the difference between the higher SI of the heart and the lower SI of the lung. The required slice shift was then obtained as the difference between this measured position and the measured position of the third navigator scan of the same perfusion measurement as the reference scan. This allowed the magnetization in the navigator region reaching a steady-state for the reference signal. The position of the subsequent measured perfusion slice was corrected for this shift by the use of real time feedback control of the scanner (real time feedback duration = 18 msec).

For perfusion image acquisition, the following measurement parameters were used: $\alpha = 18°$; TR/TE/TI = 3.5/1.7/110 msec; FOV = 380 × 285 mm^2, slice thickness = 8 mm, GRAPPA (12) with an acceleration factor of 2 and 24 reference lines.

In addition, cardiac motion that remained during the time between motion detection and readout time of the corresponding perfusion image was compensated for. This was performed by using additional prescans (n = 46) for motion detection before the perfusion measurement. The prescans consisted of two navigators separated in time by dT (cf. Fig. 1). The measured heart's position obtained from the prescans were filled in a matrix representing all possible shifts of the heart's position during the interval dT depending on the position of the heart and its motion direction compared with the reference location obtained at the beginning of the measurement. Before starting the perfusion measurement the matrix entries for each position were averaged and not measured positions were interpolated. Then, this matrix was accounted for by summarizing the measured perfusion slice shifts during the FPP–MRI measurement with the predicted shifts at the time interval dT depending on

Table 1
Relaxation Times of Phantoms Used in the In Vitro Study

	Represented tissue equivalence in vivo	T_1-Relaxation time (msec) [exp.]	T_1-Relaxation time (msec) [Lit.]
Phantom 1	Myocardium with contrast agent	243.4 ± 16.1	96 (14) (peak value)
Phantom 2	Myocardium	834 ± 47.7	880 (11)

the position of the heart and the direction of the cardiac motion compared with the reference location. The advantage of this approach lies (a) in its rapid processing speed because no other time consuming fit-algorithms are required during the FPP–MRI measurement, (b) in its solid performance and insusceptibility to trigger errors, and (c) PST with prescans can handle both cyclic and semicyclic motion produced by irregular breathing, where the latter one is more common in clinical practice.

Phantom Study

To optimize the navigator signal and to investigate the quality of PST two phantoms were used (13). One had the T_1-relaxation time equivalent to the relaxation time of myocardium (11) and the other one had the relaxation time of myocardium combined with a CA during bolus passage (14). For this purpose, water was mixed with Gd-DTPA (Magnevist, Bayer Schering AG, Berlin, Germany). The T_2-value was adapted to myocardium by using jelly gel produced by a specific amount of agar with water instead of pure water. The relaxation times of the phantoms (Table 1) were measured using a series of saturation recovery (SR)-TurboFlash measurements with 12 different saturation times for T_1 and by subsequent fitting of the simplified SR signal equation (13) to the measured SI on a region-of-interest (ROI) basis:

$$S(C) = S_0 \cdot \left(1 - a \cdot e^{-rC}\right) \quad [1]$$

where C denotes the concentration of CA. S_0 represents the SI of the pixel without additional CA, i.e., with C = 0 mmol/L and a and r are constants, which were fitted.

During the measurements with the developed sequence the navigator was placed perpendicular to the front of the measured phantom (cf. Fig. 3). Both overlapping image slices were positioned perpendicular to the navigator. To optimize the contrast between the lung and the myocardium in the navigator signal the TE of the navigator was varied in the following way: 8.6, 12.6, 16.6, 20.6, and 24.6 msec. The signal contrast of the navigator is changed for prolonged TE from pure T_1-relaxation time dependency to a ratio of T_1/T_2-relaxation time dependency. This compensates for the dependency of the CNR between the both observed tissues in the navigator signal on the concentration of CA during bolus passage for sufficient long T_2-relaxation times.

For assessment of the quality of PST, the phantom with a relaxation time comparable to that of myocardium was used. For this purpose, the image slices were positioned at one end of the phantom and then the phantom was periodically moved in the direction of the navigator manually in such a way that the phantom moved out of and into the measured slice. Thereby, the SI oscillates depending on the phantom position caused by partial volume effects produced by the changing of phantom volume per recorded voxel. The amplitude of MR signal oscillations was used as an indicator for the quality of PST. The phantom was moved manually, because this approach includes also unpredictable motion of the heart caused by the varying respiration depth and frequency. As a consequence, this approach is a better match than pure periodical movement and gives information about the PST quality more precisely for in vivo measurements. For image quality comparison, the SNR with PST and without PST were calculated.

Animal Study

With an approval of the local animal care committee, FPP–MRI was performed at rest in healthy pigs (n = 3; weight = 25–30 kg). The pigs were ventilated with supplemental oxygen, anesthetized with propofol. For sedation and analgesia, piritramide and ketamine were used in therapeutical dosages. During the perfusion measurements, CA was administered in a bolus (dosage of 0.02 mmol/kg [Gd-DTPA, Magnevist, Bayer-Schering AG, Berlin, Germany] of bodyweight) with consecutive injection of 20 mL saline water. The perfusion was measured in short-axis view of the heart. The cardiac motion was observed by navigators at the heart basis looking at the interface between heart's and lung tissue, where the lung tissue has a low SI and the heart's tissue a high SI (cf. Fig. 4). This position was chosen in previous tests monitoring TP cardiac motion in its direction directly, minimizing partial volume effects induced by the shape of the interface and measuring enough voxel of both tissues for the border detection algorithm.

The following scan protocol in combination with the developed sequence with PST was used: (1) a FPP–MRI

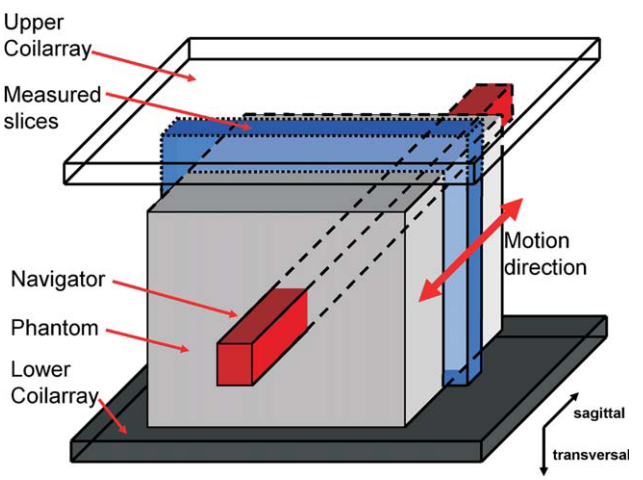

FIG. 3. Position of navigator beam and measured image slices in the phantom study. [Color figure can be viewed in the online issue, which is available at www.interscience.wiley.com.]

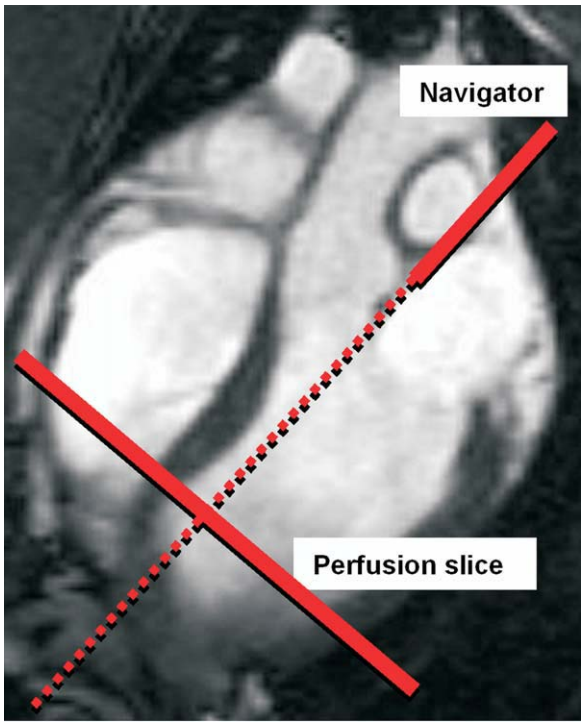

FIG. 4. Position of navigator slice in vivo detecting the interface between the heart and lung tissue at the basis of heart displayed in a four-chamber view. All perfusion measurements were performed in short axis view of the heart perpendicular to the navigator. [Color figure can be viewed in the online issue, which is available at www.interscience.wiley.com.]

measurement without prescans under free-breathing conditions; (2) a FPP–MRI measurement without prescans in a breath-hold; (3) a FPP–MRI measurement with prescans under free-breathing condition (with a delay of at least 30 min to allow for a wash-out of CA between each CA administration (15)). This protocol was applied in two pigs once and to one pig twice (with a delay of 5 h 13 min). To test whether measurements with PST are more accurate than those without, the development over time of the diameter of the left myocardium during the FPP–MRI measurement was examined as an indicator of motion (if EKG-triggering worked well) since TP motion causes changes in the diameter of the myocardium due to the almost egg-shaped left ventricle (LV). Measuring the diameter of the LV in lateral to septal direction, the average and standard deviation over time of the diameter were compared in one pig according to the protocol mentioned above.

Data Analysis of In Vivo Study

The endocardial and epicardial contours of the myocardium were manually drawn for each image to compensate for additional in-plane motion and then divided into six segments (16) for both image series of a perfusion measurement. As shown in the flowchart for data analysis of perfusion measurement in the animal study (Fig. 2), STCs were extracted for each image series by spatially averaging SI across the segments and subsequent interpolation to equidistant time intervals. The associated arterial input function (AIF) was derived from a ROI (diameter = 2 cm^2) manually drawn in the center of the LV cavity in the corresponding images. Bias by image noise was removed using the following approach:

In *k*-space, noise is normally distributed, but due to the signal magnitude reconstruction its statistical distribution becomes Rician. Moreover, it systematically changes the SI at low SNR. Gudbjartsson et al. (17) proposed an approach to correct for this effect. The relationship between the standard noise deviation in *k*-space σ and the average noise in a reconstructed image $\bar{S}_{noise}$ away from the measured object, but inside the field of view (FOV) is as follows:

$$\sigma_{noise} = \sqrt{\frac{2}{\pi}} \cdot \bar{S}_{noise} \quad [2]$$

On this basis, we obtained an approximation for the noise-free SI (S_{corr}) of a region in the examined object with the following relationship:

$$S_{corr} = \sqrt{(S^2_{uncorr} - \sigma^2_{noise})} \quad [3]$$

with S_{uncorr} being the noise signal of the same region in the object.

On this basis, Schreiber et al. (18) proposed a subsequent approach for calculating the standard deviation of noise, if temporal development of SI is known in principle. The estimated time course is adapted to the measured SI of a ROI over the duration of the measurement in an examined image sequence. This is done using a nonlinear regression analysis, and the relationship is derived from Eq. 3. This leads to with an additional constant baseline signal contribution, i.e., the SI before the arrival of CA (S_{preCA}):

$$S_{uncorr}(t) = \sqrt{((S_{fit}(t) + S_{preCA})^2 + \sigma^2_{noise})} \quad [4]$$

This approach is only valid for a gaussian noise distribution. However, in parallel imaging normal distribution of noise is generally not given. Nonetheless, Thunberg et al. (19) were able to demonstrate that noise is nearly gaussian distributed for small ROIs in images sampled with an acceleration factor of 2 and the GRAPPA (12)-algorithm for reconstruction. Hence, due to the measurement parameters for parallel imaging used in our study, the approach of noise correction as described above was considered as a valid approximation for this study.

This method of noise reduction was applied by adjusting a lognormal function (20) to the measured AIF:

$$S_{AIF}(t) = \sqrt{(S^2_{preCA} + \left[\left(\frac{A}{\sqrt{2\pi} \cdot w \cdot t}\right) \cdot \exp\left[-\left(\ln\left(\frac{t}{t_0}\right)\right)^2 \Big/ 2 \cdot w^2\right]\right]} \quad [5]$$

where A, w are fit parameters and S_{preCA} the SI before bolus arrival of CA. The fitting was done using the Levenberg-Marquardt-Minimization (Origin 7, v7.0303; OriginLab Cooperation, Northampton, MA). To avoid the influence of a second bolus passage of CA, only data points were used until SI had dropped to 30% of its

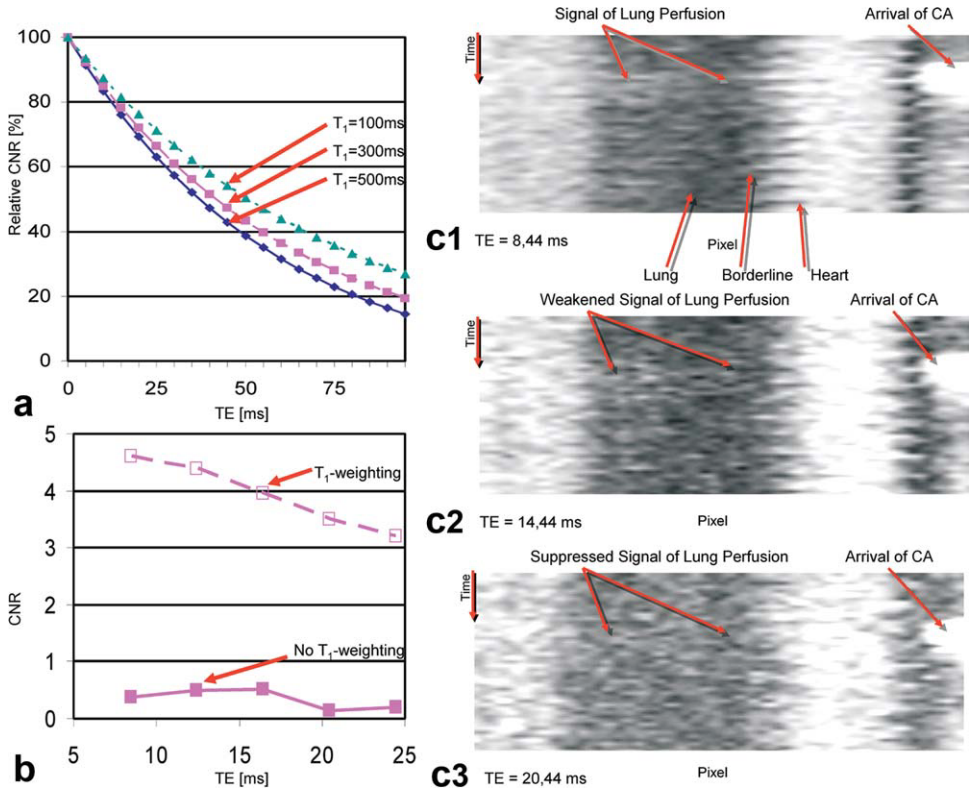

FIG. 5. CNR-dependency on TE between tissues during CA passage in the navigator signal. **a**: Simulated data: relative CNR between myocardium and tissues with several amounts of CA standardized on CNR for TE = 0 msec (TR = 460 msec; T_2 = 75 msec). Longer TE reduces CNR between tissues and therefore the dependency on T_1. **b**: Phantom measurement: for increased TE, the CNR between both phantoms is reduced. T_1-weighting of subsequent perfusion slice readout shortens TR, which increases the CNR between both phantoms in the navigator signal. **c**: In vivo data of the influence of lung perfusion on border detection. Bolus of contrast agent increases signal of lung tissue and influences the contrast of interface between heart and lung tissue for echo time (TE) = 8.44 msec as short as possible. Optimized TE decreases signal of lung perfusion, which leads to a more accurate border detection (TE = 20.44 msec). [Color figure can be viewed in the online issue, which is available at www.interscience.wiley.com.]

peak value after its peak. Also a Fermi-function (20) was adapted to STCs of segments of the myocardium using the Levenberg-Marquardt-Minimization with:

$$S_{\text{myocardium}}(t) = S_{\text{preCA}} + \left[S^{\max}_{\text{bolus}} - S_{\text{preCA}} \Big/ \left(1 + e^{\frac{(t-t_0)}{b}} \right) \right] \quad [6]$$

with S_{preCA} denoting the SI before the arrival of CA, $S^{\max}_{\text{bolus}}$ the maximum SI during passage of CA and b fit parameter. The noise corrected STCs were then calculated by:

$$S_{\text{corr}}(t) = \sqrt{\left(S^2_{\text{uncorr}}(t) - \sigma^2_{\text{noise}} \right)} - S_{\text{preCA}} \quad [7]$$

Concentration time curves (CTC) were then derived from the noise-corrected STCs using (21):

$$c_{\text{CA}}(t) = \frac{1}{-\text{TR} \cdot r_1} \ln \left[\frac{(S(t) - S_0)}{E_1 \cdot (S(t) \cdot \cos\alpha - S_0)} \right] \quad [8]$$

where $S(t)$ is the steady-state SI during the perfusion measurement, S_0 is the SI in the thermal steady state and $\alpha = 18°$, $r_1 = 4.26\ \text{mM}^{-1}\ \text{s}^{-1}$ and $E_1 = \exp(-TR/T_1)$. This equation for the calculation of the CTCs is obtained by combining the SI of the steady state of a SRTF sequence and the relaxation time T_1 influenced by CA:

$$\frac{1}{T_1} = \frac{1}{T_1^0} + r_1 \cdot c_{\text{CA}}(t) \quad [9]$$

where T_1^0 is the relaxation time without CA influence. For the analysis of the first perfusion measurement per animal the mean value $T^0_{1,\text{AIF}} = 1267 \pm 72$msec (22) and for the myocardium the mean value $T^0_{1,\text{myocardium}} = 880$msec (11) were used. The T_1-values of the following perfusion measurements were adapted by the concentration of residual CA from previous injections using Eq. 9. The residual concentration of CA was calculated by measuring the signal enhancement between the prebolus signal of the current perfusion measurement and the first one in the investigated animal using Eq. 8.

The quantitative MBF values were calculated from baseline-normalized CTCs to avoid a dependency on remaining CA from previous injections (21).

For the quantification of MBF, a two compartment model (MMID4) was used to analyze the CTCs using the algorithm SENSOP of XSIM (23,24). The two compartments comprise intravascular and interstitial extracellular space.

Data fitting was performed using XSIM with following three variable parameters and their corresponding starting

Table 2
Time Dependency of Left Myocardial Cavity Diameter During FPP-MRI Measurements In Vivo

	Average (mm)	Standard deviation (SD) (mm)	SD (with PST)/ SD (without PST)
Free-breathing			
With PST	50.23	0.83	0.40
With PST + navigator prescans	50.11	0.94	0.41
Without PST	53.11	2.06	
Breath-hold			
With PST	50.08	0.56	0.96
Without PST	50.00	0.58	

Error of measurement was 1 mm.

values: MBF = 1.0 mL/min/g within the limits 0.0–7.0 mL/min/g, the permeability surface area product (PS) = 0.5 mL/min/g within the limits of 0.25–8 mL/min/g, and the delay (D) = 0.0 sec between CA inflow in the LV cavity and the myocardium between the limits 0.0–5.0 sec (24). All other values for the distribution volumes of the CA were kept fixed as listed in the literature.

The statistical analysis of the MBF data was done using the nonparametrical Wilcoxon-signed rank test (25) (SPSS 15.0 for Windows, Version 15.0.1 (November 22, 2006), Munich, Germany). To test the equality of variance in datasets measured with and without PST the Levene's test was used. When it is significant, equality of variance is not assumed.

RESULTS

Phantom Study

Longer TE reduces the dependency on T_1 between two tissues as we shown in the simulation (cf. Fig. 5) and the phantom study (cf. Fig. 5). A sufficient reduced contrast between the investigated phantoms was found for $TE_{Navigator}$ = 20.44 msec of the navigator module compared with the CNR with the shortest possible TE_{min} = 8.44 msec. This was validated in the navigator signal in vivo, where the signal change of the lung perfusion was suppressed for the optimized TE during a perfusion measurement (Fig. 5).

Another aim of the phantom study was to measure the quality of the PST approach. The standard deviation over time of SNR, whose oscillation was caused by phantom motion, was 0.12 for the total duration of the measurement in the slowly moving phantom. It increased to 0.37 for a phantom, which was quickly moved back and forth. This increase of the standard deviation is caused by the remaining motion of the phantom during the time period (dT) between the recording of the navigator signal and the sampling of the k-space center of the corresponding perfusion image. This remaining motion may lead to a misplaced perfusion slice readout despite PST is being applied. The misplaced perfusion slice may possibly be located outside the phantom, which could change the SI of ROI in the examined phantom and also the value of the standard deviation of SI over measurement time. To compensate for remaining motion due to the continuous motion, the approach with prescans introduced above was tested to predict the motion of the k-space centerline of the corresponding perfusion image. Using this approach, the standard deviation decreased to 0.09 for an averaged oscillation speed without increasing of the calculation time of the slice shift during image acquisition and considering a complicated predictable movement of the manually moved phantom.

In Vivo Study

In vivo the optimized TE also results in an increased signal difference between lung and heart (cf. Fig. 5), especially during the bolus passage of CA, because the signal of lung perfusion of CA is suppressed and the detectability of the lung-heart interface is enhanced.

To check for the quality of PST with and without prescans, the diameter of the left myocardial cavity was measured during FPP–MRI measurements under both conditions. The mean diameter values were comparable within the range of the measurement error during observed perfusion measurements for both PST approaches in both conditions (Table 2). The standard deviations for both PST approaches under free-breathing conditions were slightly higher than those in a breath-hold, but still remained within the range of the measurement error. As expected, both the average and the standard deviation of the perfusion measurement without PST under free-breathing conditions are notably higher. This

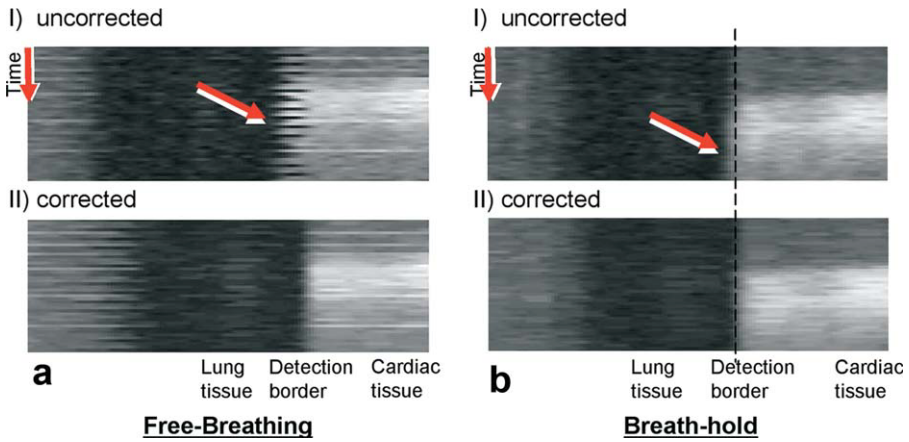

FIG. 6. Uncorrected and corrected navigator signal over time under free-breathing and breath-hold conditions for the third animal. **a**: Heart motion caused by breathing is compensated in corrected navigator signal (arrow). **b**: Offset of heart position caused by decrease of lung volume during uptake of oxygen is compensated in corrected navigator signal (arrow). [Color figure can be viewed in the online issue, which is available at www.interscience.wiley.com.]

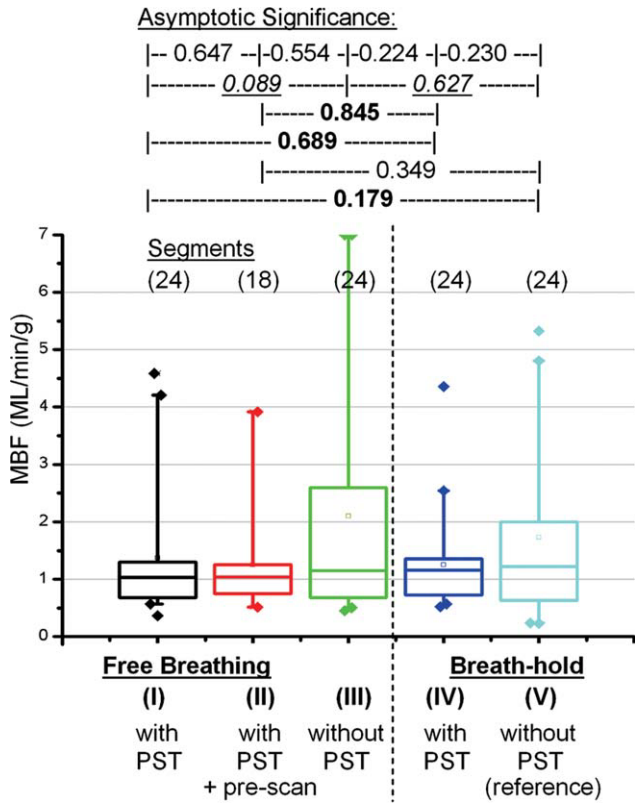

FIG. 7. Box plots of quantitative MBF values of the animal study separated in each method and condition with *P*-values from the statistical analysis (Wilcoxon-test). Percentile ranges of MBF values measured with PST are comparable under both conditions and considerably smaller than for values measured without. Median values of (I) and (II) are as predicted for healthy hearts, whereas median values of the other approaches are notably higher and the distributions are significantly ($P < 0.012$) different. [Color figure can be viewed in the online issue, which is available at www.interscience.wiley.com.]

is caused by uncompensated cardiac motion and considerable changes of the corresponding diameter changes of the left myocardium. Comparing these results with the corresponding navigator images (cf. Fig. 6), cardiac motion caused by changes of lung volume is well compensated for under free-breathing condition. This is also valid for remaining motion under breath-hold conditions, where the analysis of the LV diameter shows no difference despite the small shift over time for the FPP–MRI without PST in the corresponding navigator signals.

In the perfusion study, the protocol of the in vivo study was successfully applied in all three animals with sufficient CNR in the navigator images for cardiac motion detection, which demonstrates the practicability of FPP–MRI with navigator-based PST. Regarding MBF, PST significantly ($P = 0.012$) reduced range of the results due to cardiac motion under free-breathing condition (cf. Fig. 7 (I–III)). Even during breath-hold conditions, quantification did benefit significantly ($P = 0.011$) from PST because remaining motion (e.g., by oxygen consumption in the lung during the breath-hold) was minimized (cf. Fig. 7 (IV–V)). Comparing median MBF values measured with PST for both conditions, results obtained under breath-hold are slightly higher within the physiological range (26), but with no statistical significance (cf. Fig. 7). Its interquartile range is comparable with that under free-breathing conditions. This leads to the conclusion, that the measurements with PST under both conditions are comparable. Furthermore, the median value measured without PST under breath-hold condition is slightly higher than predicted (Table 3). For median MBF values that are separated in standard segments of myocardium (cf. Fig. 8), the approaches with PST show homogeneous behavior around the value of 1.0 mL/g/min for all segments. Without PST, median values are notably overestimated in the segments bordering the lung. This is caused by the cavity that shines through during cardiac TP motion.

DISCUSSION

In this study, we compared quantitative MBF values measured with FPP–MRI with and without PST under free-breathing and under breath-hold conditions, respectively. The PST approach was navigator-based with the navigator positioned perpendicular to the corresponding perfusion slice across the heart. The advantage of this approach is that cardiac motion is measured directly with no additional underlying model calculations connecting diaphragm and cardiac motion. In consequence, the approach presented in this study provided a more direct and straightforward way for accurate compensation of cardiac motion than the conventional approach.

As a result, we found that quantification of MBF benefits from PST under free-breathing and under breath-hold conditions. It significantly ($P = 0.012$) reduces the range of the measured MBF values under free-breathing. With PST, the shine-through of the LV and the resulting signal changes are decreased, which are caused by TP cardiac motion. This minimizes also oscillations in the derived CTCs and enhances the quality of MBF quantification. Residual in plane motion is compensated for both methods in the analysis by drawing the ROIs

Table 3
Quantitative MBF Values (mL/min/g) Measured In Vivo

	Free-breathing			Breath-hold	
	With PST	Without PST	With PST+Prescans	With PST	Without PST
Median	1.04	1.15	1.05	1.20	1.30
25% Percentile	−0.28	−0.48	−0.27	−0.44	−0.58
75% Percentile	0.30	1.10	0.20	0.15	0.71
Interquartile range	0.58	1.58	0.47	0.59	1.29

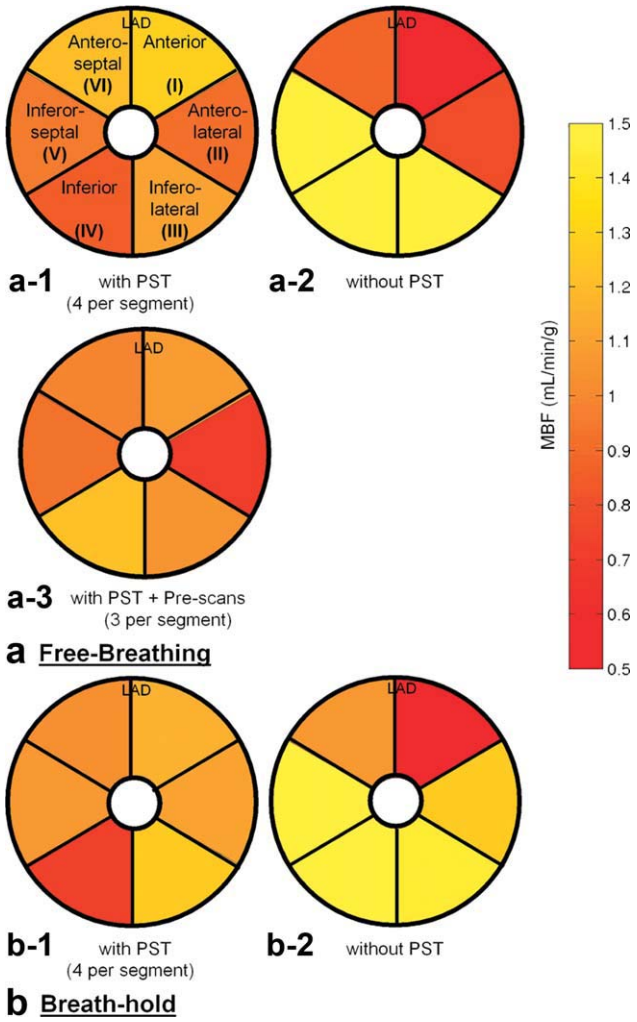

FIG. 8. Median values of quantitative MBF measurements segmented in standardized regions of left myocardium. Approaches with PST (**a-1**, **a-3**, and **b-1**) show homogeneous behavior around 1.0 mL/g/min for all segments, whereas without PST (**a-2** and **b-2**) the median values of the inferior-septal to inferior-lateral segments (III)–(V) are considerably overestimated caused by heart motion.

manually and therefore does not affect the presented results. PST also compensates significantly ($P = 0.011$) for remaining motion of the heart induced by changes of the lung volume (e.g., oxygen uptake) under breath-hold condition and therefore diminishes the signal changes due to partial volume effects. This reduces also the range of the measured MBF. The median values measured with PST approaches under free-breathing conditions were comparable with the values measured with PET in healthy myocardium (2). The median values measured under breath-hold conditions are visually but not statistically significant higher for both approaches with and without PST. It has to be proven with a larger number of subjects, if the offset of median values is a systematic error of the method of FPP–MRI in a breath-hold (e.g., caused by stress during the long, necessary breath-hold).

These results correspond well with the results found by Pedersen et al. (8) that a reduction of the TP cardiac motion improves the estimation of the myocardial perfusion notably under free-breathing conditions. In their study, the lung-diaphragm interface was observed by the standard navigator approach, which was a major source of error due to the poor SI of the navigator signal during FPP–MRI and reduced the accuracy of the motion correction. In our study, the navigator signal was sufficiently measuring cardiac motion directly (cf. Fig. 6), but it needed experience in positioning at the heart's basis for accurate compensation of cardiac motion compared with the standard approach. However, in this study for PST no underlying model had to be adapted compensating the lagged cardiac motion, and compensation of cardiac motion was more straightforward in our study.

In the study of Pedersen et al. (8), TP motion contaminates mostly free-breathing perfusion measurements in subendocardial regions. This agrees with the results of our study where the quantitative MBF values measured without PST were notably overestimated in the inferior-septal to inferior-lateral standard segments for both free-breathing and breath-hold conditions, respectively. This leads to the conclusion that TP motion mostly contaminates the inferior segments bordering to the lung independent on breathing conditions and has to be taken into account for FPP–MRI.

The next step is to test this promising approach of FPP–MRI with PST in a volunteer study with multiple injections of CA and various perfusion imaging sequences with PST in random order. A further step would be testing this approach in ischemic heart disease under free-breathing and under breath-hold conditions. This would show the quality and comparability of this approach under both conditions. Furthermore, the transfer of this approach to clinical examinations would be important, since, on one hand, it additionally reduces errors caused by breathing during image sampling under breath-hold conditions. In everyday clinical situations, this problem also has a negative influence on an accurate quantification of MBF. On the other hand, the PST under free-breathing gives a possibility to examine patients with severe cardiac diseases, whose examination is impossible nowadays due to the long time of breath-holding for a FPP–MRI measurement.

A limitation of this study was the small number of animals in the in vivo study. The insufficient coverage of the heart using only a single measured perfusion slice was introduced by the experimental design to compare measurements with and without PST at the same position within the same heartbeat; this can be changed in real clinical or experimental studies. In this sequence, more slices with PST can be measured for better covering of the heart by dropping the measurement without PST. In this case, it is recommended to apply the prescan approach for each measured slice to compensate for the increasing amount of residual cardiac motion between the navigator acquisition and the readout of each additional perfusion slice or apply the navigator module for each measured slice. Then a minimum of three perfusion slices can be measured at different positions with an acquisition time of around 200 msec for each slice with additional ~50 msec per navigator module (heartbeat rate = 800 msec). Another limitation of this study was that only motion of the heart in the TP direction was monitored and compensated for. In future

studies, more complex motion compensation should be implemented since the cardiac motion is in all three directions in space. Moreover, the feasibility of this approach has to be tested under stress conditions with its shorter duration of the heart cycle and the stronger resulting time restrictions for FPP–MRI measurements.

CONCLUSION

In conclusion, quantitative MBF values measured with PST are more accurate by reducing the variety of the obtained MBF values, which is induced by cardiac motion in breath-hold and under free-breathing conditions. Therefore, FPP–MRI measurements benefit significantly by the use of PST under both breathing conditions.

REFERENCES

1. Kaufmann PA, Camici PG. Myocardial blood flow measurement by PET: technical aspects and clinical applications. J Nucl Med 2005; 46:75–88.
2. Chareonthaitawee P, Kaufmann PA, Rimoldi O, Camici PG. Heterogeneity of resting and hyperemic myocardial blood flow in healthy humans. Cardiovasc Res 2001;50:151–161.
3. Prinzen FW, Bassingthwaighte JB. Blood flow distributions by microsphere deposition methods. Cardiovasc Res 2000;45:13–21.
4. Wilke N, Jerosch-Herold M, Stillman AE, Kroll K, Tsekos N, Merkle H, Parrish T, Hu X, Wang Y, Bassingthwaighte J. Concepts of myocardial perfusion imaging in magnetic resonance imaging. Magn Reson Q 1994;10:249–286.
5. Li D, Kaushikkar S, Haacke EM, Woodard PK, Dhawale PJ, Kroeker RM, Laub G, Kuginuki Y, Gutierrez FR. Coronary arteries: three-dimensional MR imaging with retrospective respiratory gating. Radiology 1996;201:857–863.
6. Danias PG, McConnell MV, Khasgiwala VC, Chuang ML, Edelman RR, Manning WJ. Prospective navigator correction of image position for coronary MR angiography. Radiology 1997;203:733–736.
7. Manke D, Nehrke K, Bornert P. Novel prospective respiratory motion correction approach for free-breathing coronary MR angiography using a patient-adapted affine motion model. Magn Reson Med 2003;50:122–131.
8. Pedersen H, Kelle S, Ringgaard S, Schnackenburg B, Nagel E, Nehrke K, Kim WY. Quantification of myocardial perfusion using free-breathing MRI and prospective slice tracking. Magn Reson Med 2009;61:734–738.
9. Haacke EM, Brown RW, Thompson MR, Venkatesan R. Magnetic resonance imaging: physical principles and sequence design. Wiley; 1999. p 805–808.
10. Bernstein MA, King KF, Zhou XJ. Handbook of MRI pulse sequences. Elsevier Inc.; 2004. p 630–639.
11. Manning WJ, Pennel D.J. Cardiovascular magnetic resonance. New York: Churchill Livingstone; 2001.
12. Griswold MA, Jakob PM, Heidemann RM, Nittka M, Jellus V, Wang J, Kiefer B, Haase A. Generalized autocalibrating partially parallel acquisitions (GRAPPA). Magn Reson Med 2002;47:1202–1210.
13. Weber S, Kronfeld A, Kunz RP, Fiebich M, Horstick G, Kreitner KF, Schreiber WG. Comparison of three accelerated pulse sequences for semiquantitative myocardial perfusion imaging using sensitivity encoding incorporating temporal filtering (TSENSE). J Magn Reson Imaging 2007;26:569–579.
14. Messroghli DR, Plein S, Higgins DM, Walters K, Jones TR, Ridgway JP, Sivananthan MU. Human myocardium: single-breath-hold MR T1 mapping with high spatial resolution--reproducibility study. Radiology 2006;238:1004–1012.
15. Weinmann HJ, Laniado M, Mutzel W. Pharmacokinetics of GdDTPA/dimeglumine after intravenous injection into healthy volunteers. Physiol Chem Phys Med NMR 1984;16:167–172.
16. Lang RM. Recommendation for chamber quantification: a report from the American society of echocardiography's guidelines and standards committee and the chamber quantification writing group, developed in conjunction with the European association of echocardiography, a branch of the European society of cardiology. J Am Soc Echocardiogr 2005;18:1440–1463.
17. Gudbjartsson H, Patz S. The Rician distribution of noisy MRI data. Magn Reson Med 1995;34:910–914.
18. Schreiber WG, Eberle B, Laukemper-Ostendorf S, Markstaller K, Weiler N, Scholz A, Burger K, Heussel CP, Thelen M, Kauczor HU. Dynamic (19)F-MRI of pulmonary ventilation using sulfur hexafluoride (SF(6)) gas. Magn Reson Med 2001;45:605–613.
19. Thunberg P, Zetterberg P. Noise distribution in SENSE- and GRAPPA-reconstructed images: a computer simulation study. Magn Reson Imaging 2007;25:1089–1094.
20. Schreiber WG, Schmitt M, Kalden P, Mohrs OK, Kreitner KF, Thelen M. Dynamic contrast-enhanced myocardial perfusion imaging using saturation-prepared TrueFISP. J Magn Reson Imaging 2002;16: 641–652.
21. Cleppien DE, Horstick G, Abegunewardene N, Weber S, Mueller CE, Heimann A, Kreitner KF, Kempski O, Schreiber LM. Quantification of myocardial blood flow in the presence of residual contrast agent from previous injections. In: Proceedings of the 17th Annual Meeting ISMRM, Hawaii; 2009. p 3276.
22. Cheng HL. T1 measurement of flowing blood and arterial input function determination for quantitative 3D T1-weighted DCE-MRI. J Magn Reson Imaging 2007;25:1073–1078.
23. Chan IS, Goldstein AA, Bassingthwaighte JB. SENSOP: a derivative-free solver for nonlinear least squares with sensitivity scaling. Ann Biomed Eng 1993;21:621–631.
24. Schmitt M, Horstick G, Petersen SE, Karg A, Hoffmann N, Gumbrich T, Abegunewardene N, Schreiber WG. Quantification of resting myocardial blood flow in a pig model of acute ischemia based on first-pass MRI. Magn Reson Med 2005;53:1223–1227.
25. Wilcoxon F. Individual comparisons by ranking methods. Biometrics Bulletin 1945:1:80–83.
26. Bassingthwaighte JB, Beard DA, Li Z. The mechanical and metabolic basis of myocardial blood flow heterogeneity. Basic Res Cardiol 2001;96:582–594.